Journal of Chemical&Engineering Data

pubs.acs.org/jced Article

Liquid and Dense Phase Thermal Conductivity Measurements of CO_2 + N_2 and CO_2 + CH_4 Mixtures at Temperatures from 223 K to 308 K and Pressures up to 20 MPa

Dongchan Kim, Sigurd Weidemann Løvseth,* Arash Arami-Niya, and Eric F. May

Cite This: https://doi.org/10.1021/acs.jced.1c00270 Read Online

ACCESS | Metrics & More | Article Recommendations

ABSTRACT: New data are presented for the thermal conductivity for CO_2-rich binary mixtures in the liquid and dense phase, for temperatures between 223 and 308 K and pressures up to 20 MPa. Binary mixtures with mole fractions of 5% nitrogen and 5, 10, and 20% methane were investigated. Understanding the fluid properties of CO_2-rich mixtures at relevant conditions is important for the deployment of efficient and robust systems for carbon dioxide capture and storage (CCS), but except that for water-rich CO_2 + H_2O mixtures, no thermal conductivity data on liquid or dense phase mixtures including CO_2 are known to be reported prior to this work.

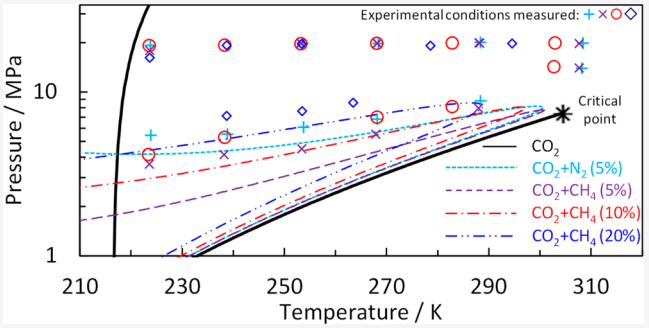

1. INTRODUCTION

Anthropogenic climate change is currently a major global challenge, and hence reducing greenhouse gas emission is a central objective for policymakers around the world. Correspondingly, to aid the governments in reaching the ambitions goals of limiting global warming to 1.5 to 2 °C, international organizations such as the International Energy Agency (IEA) and International Panel for Climate Change (IPCC) have performed thorough studies for how pathways under different scenarios could lead to the fulfilment of these goals.[1,2] A common aspect of almost all pathways is that the multitude of measures needed includes capture and permanent storage of CO_2, in quantities similar to or larger than the current natural gas market. This will require substantial infrastructure and energy consumption. It is also essential, particularly in the early phases of deployment, to ensure public acceptance and trust and avoid costly shutdowns. Hence, it is crucial to optimize the design and operations of the involved processes and systems with respect to costs, robustness, and safety. However, such optimization is only possible if the properties of the fluids involved are known under relevant conditions.

Throughout the chain, there will be other components besides CO_2, which will affect fluid properties[3] and hence the performance of different processes.[4,5] Impurities will naturally occur before the CO_2 capture and in geological storage reservoirs. Depending on the process, the impurity level in captured CO_2 products varies significantly. Impurities may have undesirable effects on the entire chain, but stringent purification could impose a high cost. Hence, although various CO_2 quality specifications[6−12] are in use and have been proposed for CO_2 transport and injection, the ideal specifications for a given system can only be found through a detailed cost optimization of all processes downstream of the capture plant. Such an optimization has to rely on detailed physical models of each process which in turn require accurate property predictions, as acknowledged by a number of reports, including the Norwegian feasibility studies on full-scale CCS.[13−16]

Unfortunately, there are currently large gaps in the property data for CO_2-rich mixtures,[17−20] which leads to correspondingly large uncertainty in property models. In a 2011 review, the IEA Greenhouse Gas R&D Programme (IEAGHG) found no viscosity or density data for mixtures relevant for geological storage conditions.[4] Unlike most natural gas processes, CO_2 processes often are operated close to the critical point, where the impact of impurities can be significant.

For injection of cold liquid CO_2 into reservoirs, thermal conductivity, λ, must be known to assess heat transfer and integrity issues of wells and reservoirs.[21−24] Thermal conductivity is also essential when designing ships for the transport of liquid CO_2 at low pressure. Additionally, viscosity and thermal conductivity play a crucial role for the performance of heat exchangers in capture and conditioning,[25] pressure drop in solvent columns,[26] adsorption, and membrane processes.[5]

Special Issue: In Honor of A. E. Mather

Received: April 15, 2021
Accepted: July 16, 2021

Table 1. Gas Mixtures Used in the Experiments[a]

	component (2)							
mixture name	chemical name	CASRN	mole fraction purity	y_2	$U(y_2)$	cylinder pressure (MPa)	source	analysis method
CN05	nitrogen	7727-37-9	0.999999	0.0493	0.0010	4.7	Coregas	none
CC05	methane	74-82-8	0.999999	0.0482	0.0010	4.7	Coregas	none
CC10				0.0988	0.0020	5.0	Coregas	none
CC20				0.1991	0.0040	5.6	Coregas	none

[a]Component (1) is carbon dioxide in all mixtures, with specifications provided in Table 2. Y_i is the mole fraction of component i, $U(Y_i)$ is its expanded uncertainty ($k = 2$), $Y_1 = 1 - Y_2$, and $U(Y_1) = U(Y_2)$.

The accepted reference correlation for thermal conductivity of pure CO_2 has for 27 years been from Vesovic et al.[27] NIST recently published a new correlation,[28] with an estimated uncertainty of 3% in the gas phase, 1% in the liquid phase, and 2−3% in the relevant supercritical region. For estimation of the thermal conductivity of mixtures, extended corresponding state models are widely used. For example, this approach is used in the REFPROP thermodynamic library[29,30] in a further development of the TRAPP[31] model. The use of the Wassiljewa-equation,[32] for example, as formulated by Mason and Saxena,[33] is another well-established method. Another approach for estimating thermal conductivity is based on excess entropy scaling.[34−39]

Currently, there are very few data on thermal conductivity for CO_2-rich mixtures, and none for the liquid phase. The corresponding large uncertainties in existing thermal conductivity models is an obstacle for cost-effective and safe design and operation of CCS processes. Hence, the ImpreCCS consortium[41] has generated data on thermal conductivity at conditions relevant for CCS to assess and improve the available models. In this work, the thermal conductivity of $CO_2 + N_2$ and $CO_2 + CH_4$ mixtures in the liquid and dense phases was measured using the transient hot-wire technique. We have previously in our lab used this method to measure thermal conductivities of a number of fluids in a wide range of conditions.[40−42] The ideal working equation and associated error corrections of the transient hot-wire apparatus are discussed. Before the measurements of mixtures, the thermal conductivity of pure CO_2 was measured to calibrate the system. The obtained data are then compared to the model predictions of Huber et al.[28]

2. EXPERIMENTAL METHODS

2.1. Investigated Fluids. As there are no data available for CO_2-rich mixtures in the liquid and dense phase, measurement of any such mixture would be of scientific significance. Consultation with the industrial partners of the projects led to the prioritization of $CO_2 + N_2$ and $CO_2 + CH_4$. Further, the industry has a need to confirm properties at operational conditions, typically with low impurity mole fractions. However, for higher relative accuracy and robust modeling, data with higher impurity content are needed. In addition, there are some technical constraints. The apparatus was designed for liquids. There is a limit to how low in density it is possible to measure with reasonable confidence, constraining the concentration of noncondensable gas in the mixture. The mole fractions were chosen based on a trade-off between these considerations. Coregas supplied the nominated mixtures with the specifications provided in Table 1. Cylinder pressures were below the dew point at expected storage temperatures for all these mixtures.

Thermal conductivity measurements were also performed on pure CO_2 for verification and calibration reasons, as CO_2 is already relatively well described.[28] The motivation will be further discussed in section 2.6. The specifications for the CO_2 used in these measurements are provided in Table 2.

Table 2. Pure Fluid Used in the Experiments

chemical name	CASRN	source	purification method	final mole fraction purity	analysis method
carbon dioxide	124-38-9	COREGAS	none	0.99995	none

2.2. Basic Principles. The transient hot-wire technique was used for the thermal conductivity measurements in this work. In this method, the fluid's thermal conductivity is determined by observing the temperature increase of a very thin metallic wire following the application of a step voltage signal. The voltage signal creates a line heat source in the fluid of essentially constant heat flux per unit length of the wire. The wire acts both as a heat source and a resistance thermometer.

The transient hot-wire method's fundamental working equation can be derived assuming an infinitely long and thin wire with zero heat capacity and infinite thermal conductivity placed in a uniform fluid of infinite dimensions. Further, the heat transfer from the wire is assumed to be purely conductive; that is, the fundamental working equation ignores convection or radiation. This working equation takes the following form:

$$\Delta T_{id}(r_0, t) = \frac{q}{4\pi\lambda} \ln\left(\frac{4\alpha t}{r_0^2 e^{\gamma}}\right), \quad \text{assuming } \frac{r_0^2}{\alpha t} \ll 1 \tag{1}$$

Here, ΔT_{id} is the change in temperature in this idealized case, q is the heat power generated per unit length of wire, λ is the thermal conductivity of the fluid at the test temperature T and pressure p. r_0 is the wire radius, t is the time from the onset of the step voltage signal, α is the thermal diffusivity, and γ is the Euler constant equal to 0.5772157. Hence, in this idealized case, the thermal conductivity can be found from the slope of temperature shift as a function of the logarithm of time.

In practice, the experimental design introduces a number of departures from the ideal solution. Therefore, essential corrections have to be made to the acquired experimental data to adjust it to the ideal model described by eq 1; that is,

$$\Delta T_{id}(r_0, t) = \Delta T_{exp}(r_0, t) + \sum_i \delta T_i \tag{2}$$

where $\Delta T_{exp}(t)$ is the temperature rise measured experimentally and $\Sigma_i \delta T_i$ is a sum of the applied corrections. Corrections to the ideal solution have been presented explicitly elsewhere[43−51] and are discussed briefly in section 3.1.

2.3. Experimental Overview. The core of the experimental apparatus consists of two 26 μm diameter anodized tantalum wires of length 57 mm and 20 mm. The wires were arranged in opposite arms of a Wheatstone bridge to eliminate the end

https://doi.org/10.1021/acs.jced.1c00270
J. Chem. Eng. Data XXXX, XXX, XXX−XXX

effects arising from axial conduction. The temperature shift was found by measuring the change in resistance difference between the two wires during a 1-s-long rectangular voltage signal. Hence, in order to find the thermal conductivity λ from eq 1, the wires must be characterized such that both the temperature shift ΔT as a function of change in resistance and heat per length q as a function of current are known.

The Wheatstone bridge is schematically shown in Figure 1. The variable resistances R_3, R_4, and R_{dummy} are set equal to 32 Ω.

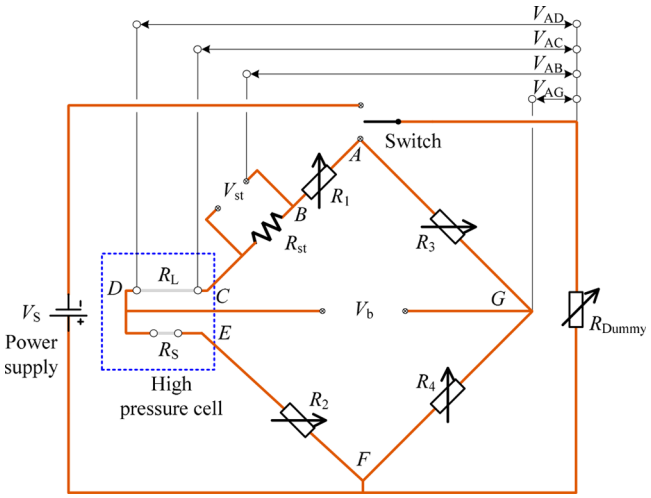

Figure 1. Schematic of the measurement Wheatstone bridge used in the current work with the supply voltage. R_1, R_2, R_3, R_4, and R_{dummy} are variable resistances, R_{st} is a standard resistance approximately equal to 10 Ω, and R_l and R_s are the resistances of the long and short sensor wires, respectively.

R_{st} is a standard resistance equal to approximately 10 Ω. R_1 and R_2 are tuned iteratively prior to each measurement using a small test supply voltage V_s for a few seconds, ensuring that the bridge is balanced, that is, that V_{br} does not change with the small nonzero V_s and that the total resistance in the measurement arm is approximately equal to the dummy resistance R_{Dummy} = 32 Ω. A measurement is triggered by a Labview program, which switches the power supply from the dummy resistance to the bridge for the duration of the rectangular voltage signal. The corresponding electric current causes heating of the long and short wires, and hence the bridge voltage V_b will increase. The Labview program controls and the data acquisition system records the voltages at B, C, D, and G at a sampling rate of 50 Hz, and hence measures the temporal evolution of both V_b and V_{st}. V_b is to the first order proportional to the change in resistance per meter wire, and hence temperature increase, while V_{st} is proportional to the current and hence to the first order to the power input per meter wire.

Figure 2 provides a schematic of the system employed, indicating the main parts of the apparatus. The two wires are placed inside a cell designed for high pressure. The cell is suspended inside an insulated liquid bath with a jacket, as shown in Figure 3. The temperature of the setup is regulated by a thermostat which circulates fluid through the jacket. Thermal uniformity is optimized by employing a stirrer in the bath (not indicated in Figure 2). Temperature is measured at the bottom of the cell as well as inside a hole on the body of the cell close to its top using 100 Ω, 4-wire, platinum resistance thermometers (PRTs). These sensors were calibrated using a standard

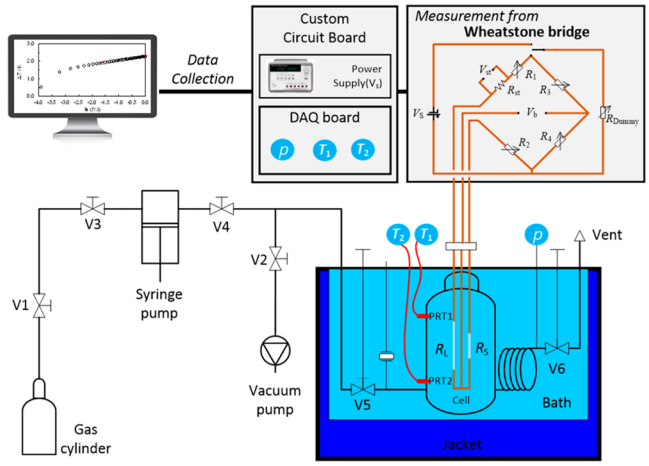

Figure 2. Simplified schematic of the transient hot-wire apparatus.

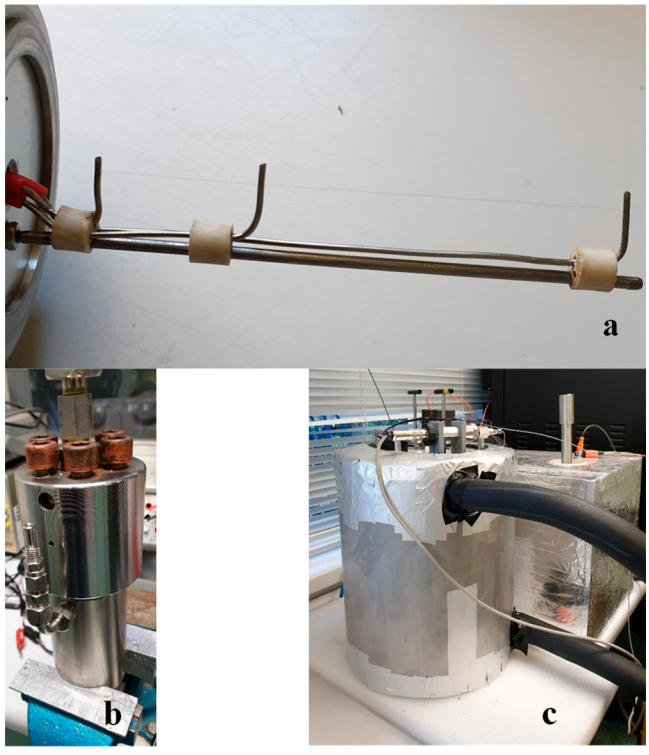

Figure 3. Tantalum wires (a), high-pressure cell (b), and insulated liquid bath with thermostated jacket (c) used in the thermal conductivity measurements.

platinum resistance thermometer (SPRT) before the measurement campaign, as discussed in section 2.5.

The cell's inlet is connected to a rupture disc, vacuum pump, and syringe pump, which again could be connected to a gas cylinder containing the gas under test. The cell's outlet is connected to drain and a 30 MPa Keller PAA-33x pressure transmitter (PT), with digital output and a specified 0.05% precision of full scale (FS), or 15 kPa. The cell can be sealed off by closing the valve at the inlet (V5), upstream from the rupture disc, and outlet (V6), downstream the pressure transducer. The RPTs and PT are logged continuously during the experimental period using a Labview data acquisition system.

2.4. Overview of Experimental Procedures. This section provides an overview of the experimental procedures, focusing

https://doi.org/10.1021/acs.jced.1c00270
J. Chem. Eng. Data XXXX, XXX, XXX−XXX

on mixtures. There was a risk of crossing into the two-phase envelope in the cell, during injection, or in the pressure transmitter at or close to ambient temperature. If no proper precautions had been made, this could have led to undetected changes in the composition of the fluid under test. With reference to Figure 2, the impact of any phase separation in the pressure transmitter was minimized by ensuring a one-way flow in the long line between the cell and V6, while the injection lines were kept at supercritical conditions as much as possible. For pure fluids or fluids and conditions where there was no danger of crossing any saturation lines, more straightforward routines could be employed.

Before the measurement, the system was evacuated. The uniform composition of gas mixtures was ensured by heating the bottom part of the cylinder to a safe but significant higher temperature than the ambient for at least 24 h. However, all mixtures were filled in the cylinders to a pressure far below the dew point and had been stored for a long time. Hence, in principle, all mixtures should already be uniform in the cylinders. After the evacuation, all valves were closed. Before injection of the gases to the syringe pump, it was ensured that both the pump and the measurement cell were at supercritical temperature with a margin of at least 10 K. For mixtures with critical point above 278 K, a low-viscosity silicon oil was hence used as thermal fluid in the setup instead of ethanol which has a flash point of 287 K.

The syringe pump was charged by opening V1, V3, and the gas cylinder valve. If charging a mixture, it was ensured that the syringe pump was set to a constant pressure mode with a set point at or above the first measurement point and well above the cricondenbar of the mixture before opening valve V4. Hence, the cell could be charged at a supercritical temperature by opening V5 while the gas line leading to the cell inlet was at a supercritical pressure. When the cell was at the desired supercritical pressure, the temperature could be changed to the first test temperature, while keeping the pump in constant pressure mode. When the cell's temperature stabilized, V4 and V5 were closed before starting the measurements, while keeping V4 open and maintaining the pump's supercritical pressure and the line between the pump and V5.

Measurements were conducted after balancing the bridge as discussed above, using an optimal supply voltage, where convection was avoided while maintaining sufficient signal strength. Several measurements were performed at each temperature, separated by at least 7 min to let the temperature profile of the cell settle.

Care was taken to avoid backflow from the pressure transmitter when there was a risk of phase separation in the line to it. Hence, in these cases, measurements were taken in decreasing order of density, as illustrated in Figure 4. In general, that meant starting at the lowest temperature and at the highest pressure of that temperature. To release pressure from the cell, either at the same temperature, or if needed when going to the next higher temperature, V6 was opened slightly while V5 remained closed, flushing the line from the outlet of the cell in the process. If the cell and the pump were at supercritical pressure, it was still possible to inject more fluid into the cell, which would be needed at 308 K/20 MPa in the example of Figure 4.

Finally, since the transient wire technique leads to heating of the fluid, typically up to a couple of degrees, care was taken when selecting experimental points close to the bubble point curve. Since there is some uncertainty in the model phase envelope predictions for the mixtures under study in this work,[51,52] a margin of 5−10 K was used on the warm side of the measurement point and at least 1 MPa in pressure.

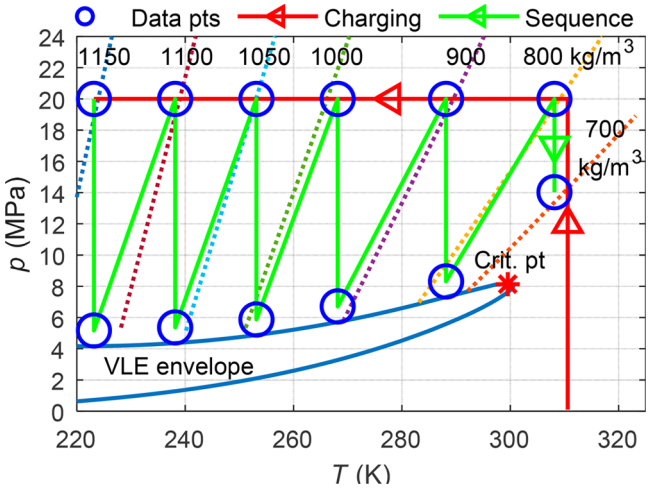

Figure 4. Planned approximate charging and measurement sequence, VLE curve, and iso-density curves for the CO_2 + N_2 mixture with 5 mol % N_2 (CN05). The thermodynamic curves are estimated using EOS-CG.[19,52−54]

For each mixture, a preliminary test matrix and measurement sequence, following the philosophy described above, was made. This experimental planning is illustrated in the case of CO_2 + N_2 in Figure 4. At supercritical conditions, the lowest pressure was limited by the values of density, viscosity, and thermal conductivity compatible with the apparatus.

2.5. Calibration of Pressure and Temperature Sensors. The 30 MPa Keller PAA-33x pressure transmitter used in this work was calibrated to traceable standards between 283 and 313 K and over the pressure span of the sensor by the supplier right before the experimental campaign. The scatter in the calibration data were well within the specified precision of 0.05% of full scale, or 15 kPa.

The 100 Ω PRTs were calibrated by bringing them together with a calibrated standard precision thermometer (SPRT) in a thermostatic bath at nine temperatures ranging from 243 to 323 K. The resistance measurements of the PRTs were fitted to a Callendar−van Dusen equation,[55] leading to an expected error of the model prediction between 243 and 308 K of the order of 10 mK or less. Below 243 K the fitted higher-order model is extrapolated, and larger errors are expected. In addition, there is uncertainty due temperature gradients in the fluid, which will be evaluated by comparing the two temperature sensors.

2.6. Characterization of Tantalum Wires. In absolute measurements, the tantalum wires must be characterized to high accuracy to calculate the thermal conductivity from eq 2, both in terms of dimensions and resistance as a function of temperature. In this work, it was instead chosen to employ relative measurements using pure CO_2 as a reference fluid. A second-degree polynomial was fitted to the temperature response of the difference in resistance between the two wires. This response was determined experimentally. A common scaling factor of the coefficients of this polynomial was fitted by comparing the model[28] and experimentally determined values of the CO_2 thermal conductivity, such that a more accurate relation between the supply voltage (proportional to q in eq 1) and bridge voltage (proportional to the experimental temperature shift, ΔT_{exp} (r_0, t) could be found.

https://doi.org/10.1021/acs.jced.1c00270
J. Chem. Eng. Data XXXX, XXX, XXX−XXX

Table 3. Overview of Thermal Conductivity Data (Experimental and Ab Initio) for CO_2 and the Binary Mixtures of CO_2 + N_2 and CO_2 + CH_4[a]

		no. sources			data ranges		
system	G/L	total	1975→	no. points	T /K	p /MPa	x_{CO2}
CO_2[b]	G/L	90	20		150−2000	0−196	1
CO_2 + N_2	G	12	2	452[c]	150−2000	0−304	0.1−0.9
CO_2 + CH_4	G	6	5	534	150−1200	0−12	0.075−0.88

[a]Including information about their phase (G, gas/supercritical phase; L, liquid) and ranges in temperature (T), pressure (p), and composition (x_{CO2}). [b]Summarized from ref 28. [c]Partly deduced from ref 18.

Table 4. Thermal Conductivity Data for CO_2 + N_2 Binary Mixtures[a]

first author	G/L	E/AI	ref	year	no. points	T /K	p /MPa	x_{CO2}
Crusius	G	AI	60	2018	173	150−2000	0	0.10−0.90
Johns	G	E	61	1988	81	322−474	1.1−31	0.29−0.84
Barua	G	E	62, 63	1968		273−573		
Gilmore	G	E	64	1966	24	348	0.1−304	0.20−0.80
Westenberg	G	E	65	1962	25	300−1100		
Cheung	G	E	66	1962		373−913		
Vines	G	E	67	1960	5	<1173		
von Lehmann	G	E	68	1957		273−623		
Kulakov	G	E	69	1955		338−1047	0.1	
Rothman	G	E	70, 71	1954/5	38	642−961	0−0.1	0.17−0.75
Davidson	G	E	72	1953	3	273	0.1	0.33−0.75
Keyes	G	E	73, 74	1951/2	22	273−623	0.1−8.5	

[a]Including information on their phase (G, gas/supercritical phase; L, liquid), generation (E, experimental; AI, ab initio), and ranges in temperature (T), pressure (p), and composition (x_{CO2}). The information is partly collected from Li et al.[18] and NIST ThermoLit.[59]

The apparatus has previously been verified with toluene and water,[40] but the properties of liquid CO_2 are closer to those of the mixtures under study. Hence, CO_2 was the preferred reference fluid for the measurements of this work.

3. ANALYSIS AND THEORY

The software estimates the evolution of the temperature $\Delta T_{exp}(r_0, t)$ and supplied heat q based on the recorded data, following the methodology, described elsewhere, for example, in ref 51. The initial part of the curve deviates from eq 1 as the assumptions used to derive it are not valid as $t \to 0$. The thermal conductivity λ is then found in an iterative manner, where repeatedly the updated estimation of λ based on eqs 1−2 is followed by an application of the corrective terms as listed below until the value of λ stabilizes. The model of Chichester and Huber implemented in REFPROP[29,30] is used to calculate the initial value of λ in this iteration

3.1. Corrections. The following corrections were considered in this work, and except for the radiative corrections, all were applied in the final data processing:

i. Finite wire heat capacity correction:[43,44,56]

$$\delta T_W(r_0, t) = \frac{q}{4\pi\lambda}\left\{\frac{r_0^2[(\rho C_p)_W - \rho C_p]}{2\lambda t}\ln\left(\frac{4\alpha t}{r_0^2 e^{\gamma}}\right) - \frac{r_0^2}{2\alpha t} + \frac{r_0^2}{2\alpha_W t} - \frac{\lambda}{2\lambda_W}\right\} \quad (3)$$

Equation 1 does not take into account the finite heat capacity of the wire, and this must be compensated by eq 3, which again is valid for thin wires, $r_0^2/\alpha t \ll 1$. α_W, λ_W, and $(\rho C_p)_W$ are the thermal diffusivity, thermal conductivity, and heat capacity per volume of the wire.

ii Outer boundary:[57]

$$\delta T_{OB}(r_0, t) = \frac{q}{4\pi\lambda}\left\{\ln\left(\frac{4\alpha t}{b^2 e^{\gamma}}\right) + \sum_{\nu=1}^{\infty} e^{-g_\nu^2 \alpha t/b^2}[\pi Y_0(g_\nu)]^2\right\} \quad (4)$$

A premise for eq 1 is an infinite outer boundary. In practice, the inner cell radius and hence the outer boundary of the heat conduction problem is finite, and eq 4 provides a correction, assuming b ≫ r_0 and (again) $r_0^2/\alpha t \ll 1$. Here, Y_0 is the zeroth order Bessel function of the second kind, while the values of g_ν are consecutive roots of the zeroth order Bessel function of the first kind, $J_0(g_\nu) = 0$. Healy et al. concluded that this correction is not significant when $b^2/at > 5.78$,[44] which has proved to always be the case in our measurements.

iii Radiation in an absorbing medium:[48,58]

$$\delta T_R(r_0, t) = -\frac{qB}{4\pi\lambda}\left[\frac{r_0^2}{4\alpha}\ln\left(\frac{4\alpha t}{r_0^2 e^{\gamma}}\right) + \frac{r_0^2}{4\alpha} - t\right] \quad (5)$$

The ideal solution assumes no radiation. As seen from the equation above, radiation manifests itself through a term in the temperature shift which is linear in time. The factor B, which requires a range of different properties of the fluid to be calculated directly, can hence be found by fitting a linear term to the temperature function, ΔT_{corr}, after the corrections have been applied:

$$\Delta T_{corr} = C_1 \ln(t) + C_2 t + C_3 \quad (6)$$

Hence, B can be found from eqs 5 and 6:

https://doi.org/10.1021/acs.jced.1c00270
J. Chem. Eng. Data XXXX, XXX, XXX−XXX

Table 5. Identified Thermal Conductivity Data for CO_2 + CH_4 Binary Mixtures[a]

first author	G/L	E/AI	ref	year	no. points	T/K	p/MPa	x_{CO2}
Hellmann	G	AI	75	2016	25	150−1200	0	0.20−0.80
Pátek	G	E	76	2005	180	300−427	0.7−12	0.25−0.75
Yorizane	G	E	77	1983	62	298−308	0.1−9	0.075−0.88
Kestin	G	E	78	1982	33	301	0.9−6.3	0.51−0.74
Christensen	G	E	79	1979	14	228−433	0.3−1.5	0.49
Rosenbaum	G	E	80	1969	220	333−433	3.3−6.9	0.24−0.76

[a]Including information on their phase (G, gas/supercritical phase; L, liquid), generation (E, experimental; AI, ab initio), and ranges in temperature (T), pressure (p), and composition (x_{CO2}).

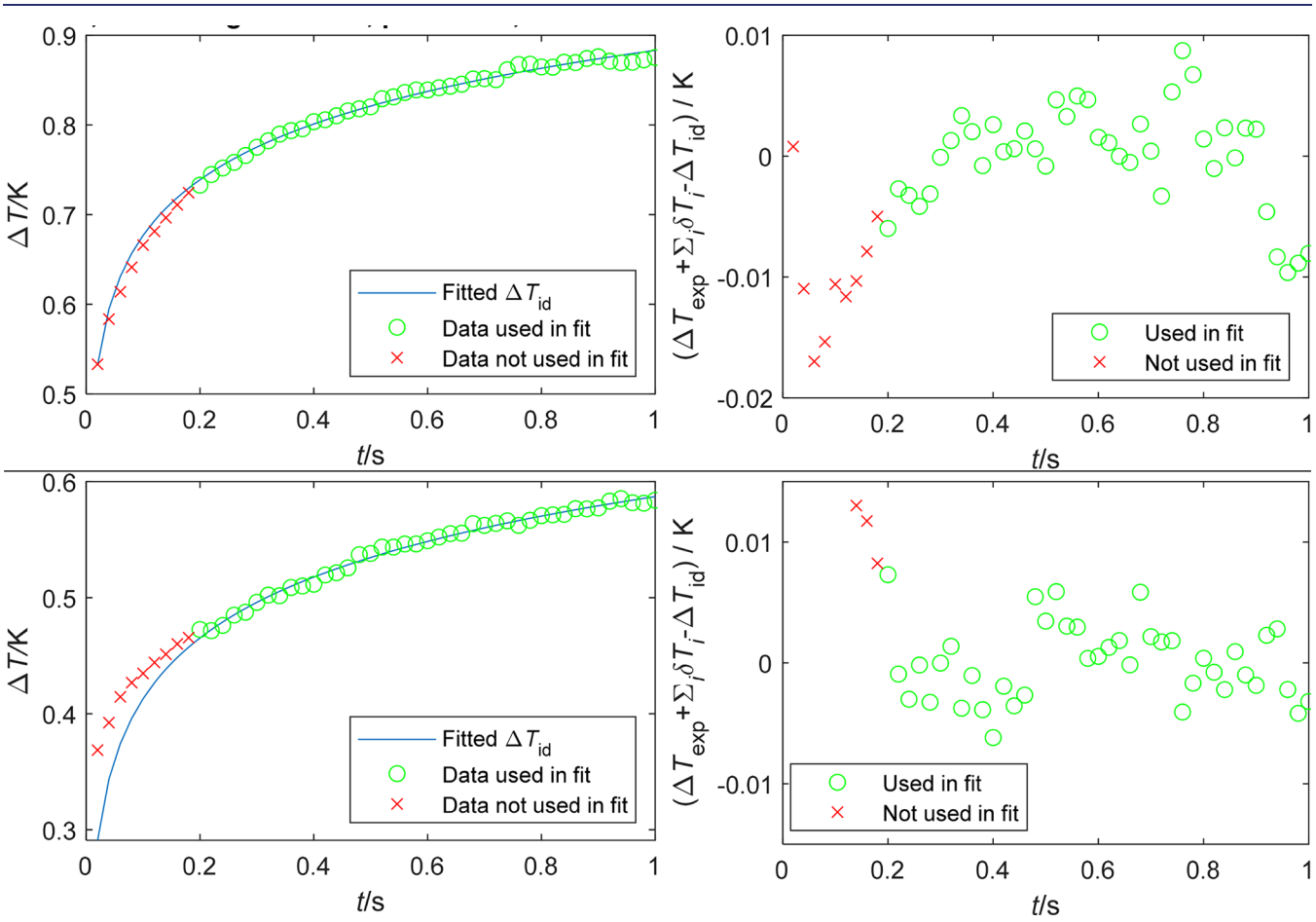

Figure 5. Two measurement samples, both for the CN05 mixture at 268 K and 20 MPa. The measurement of the upper graphs was discarded due to indications of convection, while the measurement of the lower graphs, using a lower supply voltage, was accepted. Left graphs: Measured and fitted temperature shifts as a function of time. Right graphs: Deviations between measurements plus corrections and the fitted ΔT_{id}.

$$B = \frac{-4\pi\lambda C_2}{q} \quad (7)$$

The radiative correction was applied in the initial analysis of the data. However, the estimation of B turned out to be quite sensitive to spurious measurements in the time trace, and adding ΔT_{corr} to the temperature function was seen to amplify noise to a level far beyond the anticipated impact of radiation. This correction was hence omitted when producing the data of this work.

iv Temperature shift:[44]

$$T_r = T_0 + \frac{\Delta T(t_1) + \Delta T(t_2)}{2} \quad (8)$$

As the temperature shifts up to a few degrees, this must be compensated for, both with regards to estimation of the thermophysical properties used to calculate the thermal conductivity from (2), but also with regards to the temperature which the resultant thermal conductivity measurement refers to. In eq 8, t_1 is the starting time and t_2 is the ending time of the temperature curve segment considered in the analysis, T_0 is the initial/logged temperature, whereas T_r is the temperature associated with the measurement. This is a simple correction, which will not be accurate in areas where properties are changing rapidly with temperature, that is, close to the critical point or if the temperature shift is large.

https://doi.org/10.1021/acs.jced.1c00270
J. Chem. Eng. Data XXXX, XXX, XXX−XXX

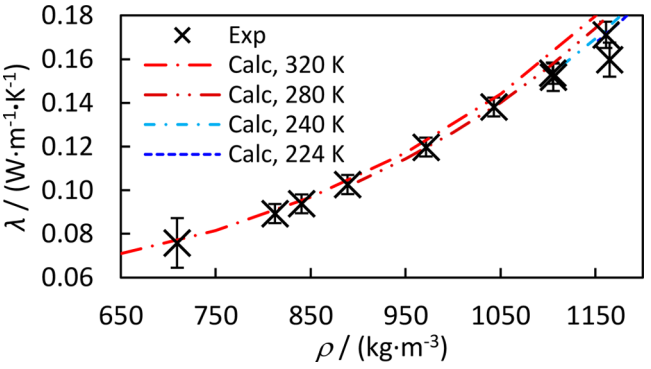

Figure 6. Response of thermal conductivity setup for pure CO_2 ("Exp") at different conditions with experimental parameters fitted to the thermal conductivity model of Huber et al.[28] plotted as a function of density using the Span-Wagner EOS.[53] Error bars indicate estimated experimental uncertainty, using a coverage factor of $k = 2$. Thermal conductivity isotherms from Huber et al.[28] are also plotted ("Calc").

4. RESULTS

4.1. Existing Data. As was seen from the surveys of refs 18 and 20, the data situation for CO_2-rich mixtures' thermal conductivity is not good. Except for CO_2−H_2O, no data were identified for CO_2-rich mixtures in the liquid phase, and the measurements for CO_2−H_2O are all old, with most of them being from the 1950s. Although there are no identified literature data that have overlap with the liquid and dense state mixture measurements of the present work, a more detailed overview of existing experimental and ab initio data in the vapor phase for the binary systems CO_2 + N_2 and CO_2 + CH_4 is provided in Tables 3−5.

A comprehensive experimental study and literature review were recently completed by NIST on pure CO_2.[28] The model provided in the same article is expected to reflect the reliable data investigated there in a good way, so this model is used as a reference in this work.

4.2. Operationalization of the Measurement Procedure. A number of measurements were made at each temperature, pressure, and composition combination. Unfortunately, there was significant noise in the bridge voltage measurements, which led to a considerable scatter in each sample's estimated thermal conductivity. It is speculated that this noise was due to EMF from an unknown source or from the data acquisition system itself.

At the same time, there is a limit to the achievable signal strength in practice. For high supply voltages, and hence measured bridge voltages, the heat transfer will be dominated by free convection, which will lead to systematic overestimation of the thermal conductivity. Free convection can be identified in a measurement by a negative curvature in the deviation plot between the measured temperature plus corrections and the fitted temperature function as a function of time, that is, by a comparison between the right and left side of eq 2. An example of evident convection, which led to a rejection of the measurement sample, is shown in Figure 5. An accepted measurement at the same conditions with lower supply voltage is also shown. The relative scatter is a bit higher, but there is no significant negative curvature in the deviation plot. The onset of convection depends on thermophysical properties such as density, viscosity, heat capacity, and thermal conductivity, of which density seems to be the most important parameter in practice.

The experimental strategy to overcome these challenges consisted of finding an ideal supply voltage on a trial-and-error basis for each investigated state, aiming for a tantalum wire heating power low enough to provide sufficient signal-to-noise ratio while avoiding convection.

4.3. Data Reduction and Uncertainty. Following the measurements, each individual trace was carefully examined. Apart from convection, an additional identified issue during the analysis was that the initial nonlinear transient of the traces had different durations. Different techniques, such as individually defining the starting point of the linear part of the trace through numerical analysis or visual inspection, was attempted. In the end, it was seen that the most repeatable results were achieved by finding the slope of the ΔT_{exp} vs the logarithm of time in a fixed time interval (from 0.2 to 1 s), while rejecting any samples that had signs of convection or where the initial transient had propagated into this interval. This was not a straightforward task, as the noise often was of the same magnitude and sometimes with characteristic frequency of ∼1 Hz.

Table 6. Experimental Measurements of Thermal Conductivity ($\bar{\lambda}$) of CO_2 in the Liquid or Dense Supercritical Single Phase as a Function of Pressure ($\bar{p}$) and Temperature ($\bar{T}$), with the Thermal Response of the Tantalum Wires Fitted to the Correlation of Huber et al.[a,28]

ID	$\bar{T}$ / K	$\bar{p}$ / MPa	$\bar{\lambda}$ / W·m^{-1}·K^{-1}	$U(\bar{T})$ / K	$U(\bar{p})$ / MPa	$U(\bar{\lambda})$ / W·m^{-1}·K^{-1}	$\lvert\bar{\lambda} - \bar{\lambda}_{calc}\rvert$ / W·m^{-1}·K^{-1}
CO2-01	223.56	4.204	0.171	0.68	0.015	0.006	0.0003
CO2-02	223.73	6.126	0.160	0.68	0.015	0.008	0.0130
CO2-03	238.75	5.029	0.152	0.11	0.015	0.006	0.0020
CO2-04	239.56	5.869	0.154	0.10	0.015	0.005	0.0000
CO2-05	253.13	4.494	0.138	0.07	0.015	0.004	0.0022
CO2-06	268.45	5.466	0.120	0.03	0.015	0.004	0.0011
CO2-07	283.66	6.976	0.103	0.03	0.015	0.004	0.0005
CO2-08	298.63	11.845	0.094	0.02	0.015	0.004	0.0002
CO2-09	308.47	14.973	0.089	0.02	0.015	0.004	0.0006
CO2-10	322.40	15.133	0.076	0.03	0.015	0.011	0.0009

[a] $\bar{T}$, $\bar{p}$, and $\bar{\lambda}$ are the mean measured temperature, pressure, and thermal conductivities. $U(\bar{T})$ and $U(\bar{p})$ are the expanded estimated uncertainties of the temperature and pressure measurements, respectively. $U_c(\bar{\lambda})$ is the estimated combined expanded uncertainty of the thermal conductivity measurements. The expanded uncertainty estimates are provided with a coverage factor of $k = 2$. $\lvert\bar{\lambda} - \bar{\lambda}_{calc}\rvert$ is the absolute difference between measured and calculated thermal conductivity value.

https://doi.org/10.1021/acs.jced.1c00270
J. Chem. Eng. Data XXXX, XXX, XXX−XXX

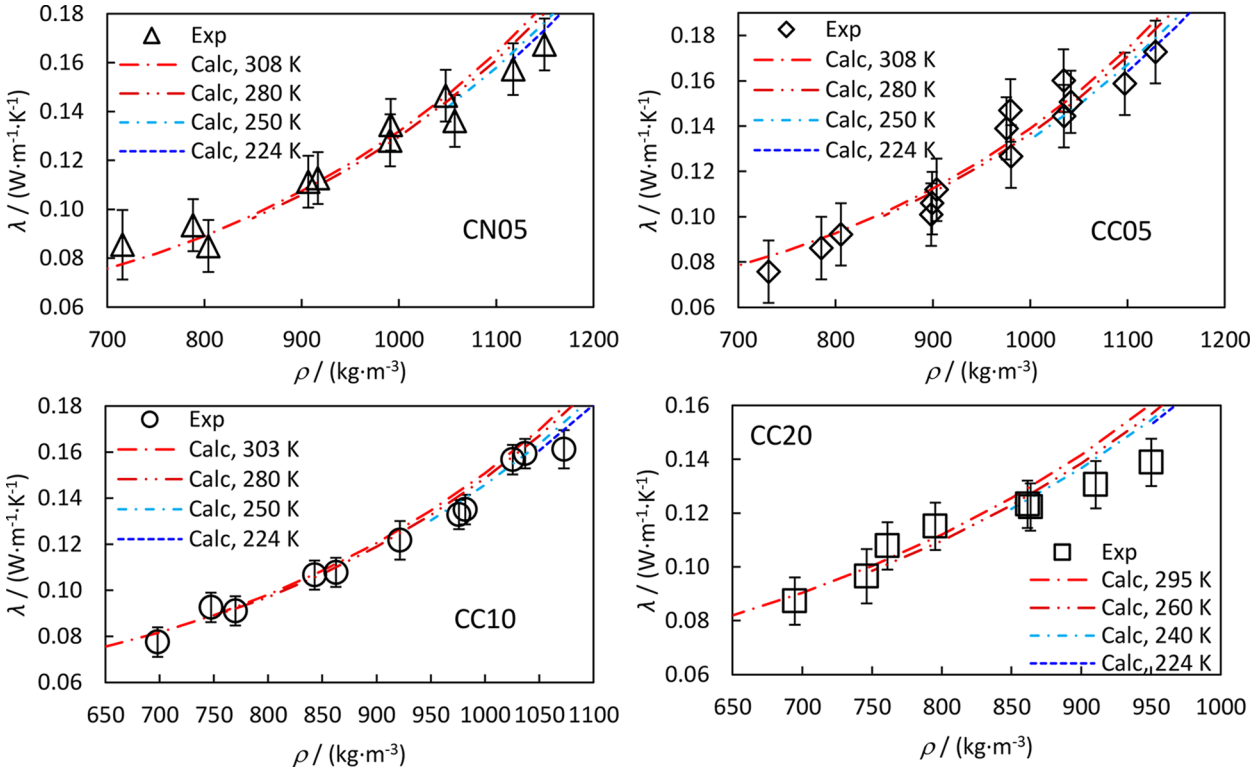

Figure 7. Measurements of thermal conductivity of four different mixtures at different conditions (Exp) as a function of density of the mixtures calculated from EOS-CG.[19,52−54,82,83] Error bars indicate estimated experimental uncertainty, using coverage factor of $k = 2$. In the same graphs selected estimated isotherms calculated using REFPROP are also shown (Calc). CN05: $CO_2 + N_2$ mixture with an approximate N_2 mole fraction of 5%. CC05, CC10, and CC20: $CO_2 + CH_4$ mixtures with CH_4 mole fractions of 5, 10, and 20%, respectively.

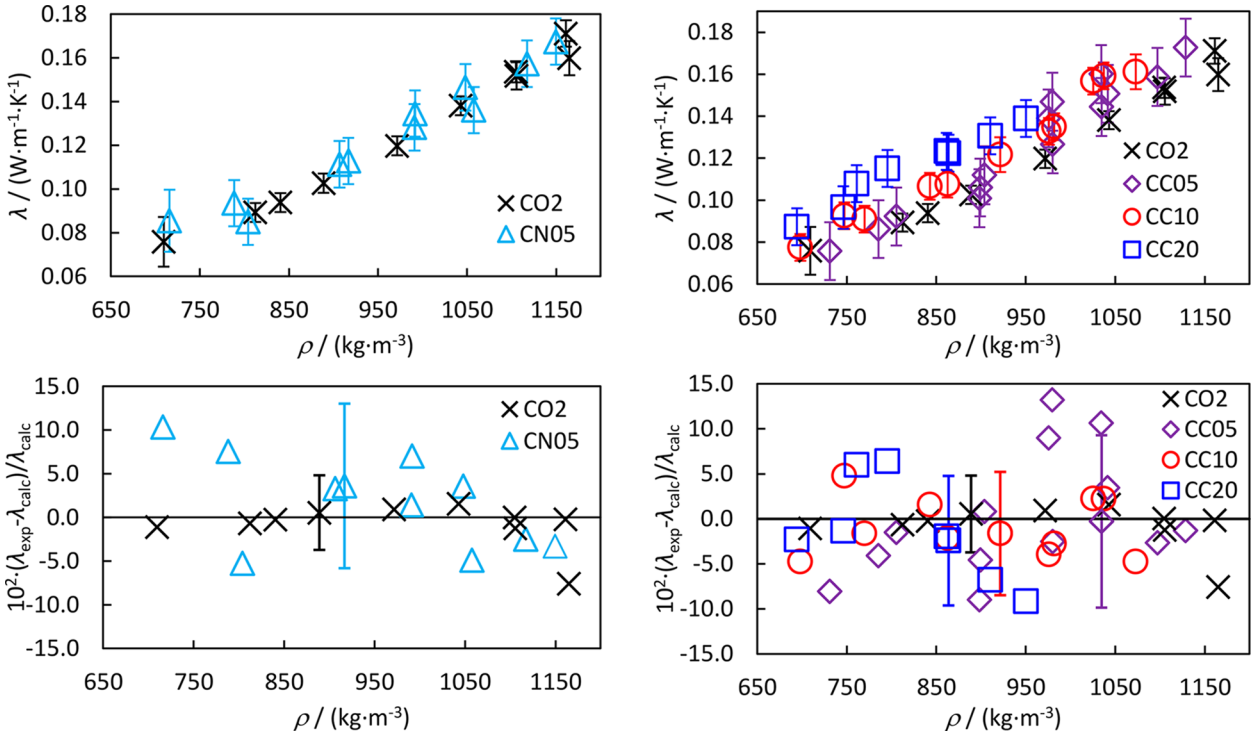

Figure 8. Measurements of thermal conductivity of CO_2 and four different mixtures at different conditions as a function of density of the mixtures calculated from EOS-CG.[19,52−54,82,83] Error bars indicate estimated experimental uncertainty, using coverage factor of $k = 2$. Left: CO_2 and $CO_2 + N_2$ mixture with an approximate N_2 mole fraction of 5%. Right: CO_2 and $CO_2 + CH_4$ mixtures with CH_4 mole fractions of 5, 10, and 20%, respectively. Top: Absolute thermal conductivity. Bottom: Relative deviations from correlations used in REFPROP.[28−30] In the deviation plots, an error bar for clarity is provided only for one representative point for each fluid.

https://doi.org/10.1021/acs.jced.1c00270
J. Chem. Eng. Data XXXX, XXX, XXX−XXX

Table 7. Thermal Conductivity Measurements of CO_2 (1) Mixed with Nitrogen or Methane (2)[a]

ID	comp	x_2	$\overline{T}$	$\overline{p}$	$\overline{\lambda}$	$U(x_2)$	$U(\overline{T})$	$U(\overline{p})$	$U_c(\overline{\lambda})$	$\lvert\overline{\lambda} - \overline{\lambda}_{calc}\rvert$
	(2)		K	MPa	$W \cdot m^{-1} \cdot K^{-1}$		K	MPa	$W \cdot m^{-1} \cdot K^{-1}$	$W \cdot m^{-1} \cdot K^{-1}$
CN05-01	N_2	0.0493	223.79	19.326	0.167	0.0010	0.67	0.016	0.011	0.006
CN05-02	N_2	0.0493	223.87	5.458	0.157	0.0010	0.67	0.015	0.011	0.004
CN05-03	N_2	0.0493	238.86	5.536	0.136	0.0010	0.11	0.015	0.011	0.007
CN05-04	N_2	0.0493	253.62	19.811	0.147	0.0010	0.07	0.015	0.011	0.005
CN05-05	N_2	0.0493	253.79	6.101	0.135	0.0010	0.07	0.015	0.011	0.009
CN05-06	N_2	0.0493	268.19	6.816	0.113	0.0010	0.02	0.015	0.011	0.004
CN05-07	N_2	0.0493	268.40	19.789	0.128	0.0010	0.04	0.015	0.011	0.002
CN05-08	N_2	0.0493	288.39	20.152	0.111	0.0010	0.02	0.015	0.011	0.004
CN05-09	N_2	0.0493	288.39	8.862	0.094	0.0010	0.02	0.015	0.011	0.007
CN05-10	N_2	0.0493	308.23	13.991	0.086	0.0010	0.02	0.015	0.014	0.008
CN05-11	N_2	0.0493	308.36	19.914	0.085	0.0010	0.02	0.015	0.011	0.005
CC05-01	CH_4	0.0482	223.58	3.621	0.159	0.0010	0.67	0.015	0.014	0.005
CC05-02	CH_4	0.0482	223.68	17.951	0.173	0.0010	0.67	0.016	0.014	0.003
CC05-03	CH_4	0.0482	238.17	4.136	0.151	0.0010	0.10	0.015	0.014	0.005
CC05-04	CH_4	0.0482	253.29	19.936	0.144	0.0010	0.05	0.015	0.014	0.001
CC05-05	CH_4	0.0482	253.33	19.818	0.160	0.0010	0.06	0.015	0.014	0.015
CC05-06	CH_4	0.0482	253.38	4.508	0.139	0.0010	0.05	0.015	0.014	0.011
CC05-07	CH_4	0.0482	267.94	5.535	0.112	0.0010	0.03	0.015	0.014	0.001
CC05-08	CH_4	0.0482	268.16	19.970	0.127	0.0010	0.03	0.015	0.014	0.004
CC05-09	CH_4	0.0482	268.20	19.844	0.147	0.0010	0.03	0.015	0.014	0.017
CC05-10	CH_4	0.0482	288.03	7.972	0.086	0.0010	0.02	0.015	0.014	0.004
CC05-11	CH_4	0.0482	288.05	19.986	0.106	0.0010	0.02	0.015	0.014	0.005
CC05-12	CH_4	0.0482	288.22	19.905	0.101	0.0010	0.02	0.015	0.014	0.010
CC05-13	CH_4	0.0482	307.72	19.845	0.092	0.0010	0.02	0.015	0.014	0.002
CC05-14	CH_4	0.0482	307.72	14.055	0.076	0.0010	0.02	0.015	0.014	0.007
CC10-01	CH_4	0.0988	223.51	4.146	0.159	0.0020	0.68	0.015	0.006	0.004
CC10-02	CH_4	0.0988	223.58	19.265	0.161	0.0020	0.68	0.016	0.008	0.008
CC10-03	CH_4	0.0988	238.43	19.318	0.157	0.0020	0.10	0.015	0.006	0.004
CC10-04	CH_4	0.0988	238.36	5.269	0.135	0.0020	0.10	0.015	0.006	0.004
CC10-05	CH_4	0.0988	253.28	19.773	0.133	0.0020	0.06	0.015	0.006	0.006
CC10-06	CH_4	0.0988	268.12	19.785	0.122	0.0020	0.03	0.015	0.008	0.002
CC10-07	CH_4	0.0988	268.17	7.016	0.107	0.0020	0.03	0.015	0.006	0.002
CC10-08	CH_4	0.0988	282.90	19.926	0.108	0.0020	0.02	0.015	0.006	0.002
CC10-09	CH_4	0.0988	282.86	8.143	0.093	0.0020	0.02	0.015	0.006	0.004
CC10-10	CH_4	0.0988	302.80	14.240	0.078	0.0020	0.02	0.015	0.006	0.004
CC10-11	CH_4	0.0988	303.03	19.899	0.091	0.0020	0.02	0.015	0.006	0.002
CC20-01	CH_4	0.1991	223.67	16.231	0.139	0.0040	0.67	0.02	0.009	0.014
CC20-02	CH_4	0.1991	238.66	19.342	0.131	0.0040	0.10	0.016	0.009	0.010
CC20-03	CH_4	0.1991	238.68	7.142	0.122	0.0040	0.10	0.015	0.009	0.003
CC20-04	CH_4	0.1991	253.41	19.666	0.123	0.0040	0.05	0.015	0.009	0.003
CC20-05	CH_4	0.1991	253.52	7.646	0.115	0.0040	0.05	0.015	0.009	0.007
CC20-06	CH_4	0.1991	263.49	8.632	0.097	0.0040	0.03	0.015	0.009	0.001
CC20-07	CH_4	0.1991	278.57	19.183	0.108	0.0040	0.02	0.015	0.009	0.006
CC20-08	CH_4	0.1991	294.60	19.853	0.087	0.0040	0.02	0.015	0.009	0.002

[a] x_2 is the mole fraction of component (2). $\overline{T}$, $\overline{p}$, and $\overline{\lambda}$ are the mean measured temperature, pressure, and thermal conductivities, respectively. The fluids under test were in the liquid or dense supercritical single phase. $U(x_2)$, $U(\overline{T})$, and $U(\overline{p})$ are the expanded estimated uncertainties of the component (2) mole fraction and the temperature and pressure measurements, respectively. $U_c(\overline{\lambda})$ is the estimated combined expanded uncertainty of the thermal conductivity measurements. The expanded uncertainty estimates are provided with a coverage factor of $k = 2$. $\lvert\overline{\lambda} - \overline{\lambda}_{calc}\rvert$ is the absolute difference between measured and calculated thermal conductivity value, using the mixture correlations provided by REFPROP.[29,30]

During this process, it was decided to discard all data with density less than 650 kg/m^3, as well as measurements of a CO_2 + N_2 mixture with 40% N_2 content, as the supply had to be turned down so much for these mixtures to avoid convection that the signal drowned in noise.

Following the analysis and selection of each ΔT_{exp} curve, the resultant measurements of acceptable quality for each point in pressure, temperature, and composition were averaged, and the uncertainty was estimated. Following the methodology described in GUM,[81] the total uncertainty was estimated by combining contributions from different independent sources, such as systematic errors from temperature, voltage, and pressure measurements, nonuniformity of the temperature measurements, and random errors (noise) on a root sum square basis.

In practice, the random scatter in the data proved to be an overwhelming dominating source of uncertainty. The estimates

https://doi.org/10.1021/acs.jced.1c00270
J. Chem. Eng. Data XXXX, XXX, XXX−XXX

take into account both deviations from sample to sample as well as long-term fluctuations over the measurement campaign.

4.4. Measurements of Pure CO_2. The measurements of pure CO_2 are plotted in Figure 6 as a function of estimated density ρ from the Span-Wagner EOS,[53] and the data are provided in Table 6. As discussed in section 2.6, the thermal response was fitted to the thermal conductivity reference correlation for pure CO_2 by Huber et al.[28] After the fit, the standard estimated error of the data vs the model is around 4%, leading to an expanded uncertainty of the fit of around 2% with a coverage factor equal to two. This uncertainty is twice the stated uncertainty value of the pure CO_2 correlation in the liquid region.[28]

Since a parameter used to calculate the data is fitted to the model, this work provides no additional confirmation of the absolute thermal conductivity value of pure CO_2. However, as seen in Figure 6, there does not appear to be a systematic trend in the deviations between the model and data. The estimated expanded combined uncertainties of the measurements with a coverage factor of $k = 2$ are indicated by the error bars in Figure 6, and these uncertainties are also provided in Table 6 together with the absolute deviations with the correlation of Huber et al.[28] For the data at temperatures of 308.5 K and below, the estimated expanded relative uncertainty is between 3 and 5%, but it is 15% at 322 K. As discussed above, this latter higher uncertainty is most likely due to the low density at that temperature. The fit is weighted with respect to the uncertainty of each data point. The temperature and pressure uncertainties have no significant impact on the combined uncertainty of the thermal conductivity, but the numbers are nevertheless included in Table 6. The increase in uncertainty of the lowest temperature is mainly due to temperature gradients of the cell.

4.5. Mixture Data. The measured data and their expanded uncertainties of the mixtures are plotted in Figure 7 as a function of density together with some thermal conductivity isotherms for the different mixtures estimated using REFPROP.[29,30] In Figure 8, the data of the different mixture systems are compared with pure CO_2. In the bottom half of the figure, the deviations between the data and the calculated values from REFPROP[28−30] are provided. The measured temperature, pressure, and thermal conductivities of the mixture data points, with corresponding uncertainties, are provided in Table 7. In the table, also the absolute thermal conductivity deviations between the data and the REFPROP[30,31] model estimates are provided. The uncertainties in composition and, like for pure CO_2, in temperature and pressure do not provide a significant contribution to the overall uncertainty of the experiment. Hence, only the combined uncertainty estimates are provided for the thermal conductivity.

Overall, the relative uncertainty of the data increases with decreasing density. Within the experimental uncertainty, there is an agreement between the model for the mixture and the measurements, with the thermal conductivity increasing with impurity content.

5. CONCLUSIONS

The first measurements of liquid and dense phase thermal conductivity of CO_2 rich mixtures with other components than water are provided. Such data will be important for the optimization in terms of design and operational strategies of the large infrastructure needed for CCS in the future.

Within experimental uncertainty, there is good agreement between the data and the corresponding state model currently used in REFPROP.[29,30] However, there is improvement potential with regards to the accuracy of the data, and there is still much experimental ground to cover for the systems investigated in the current paper, as well as for other relevant mixtures systems that currently have no data.

AUTHOR INFORMATION

Corresponding Author

Sigurd Weidemann Løvseth − *SINTEF Energy Research, NO-7465 Trondheim, Norway;* orcid.org/0000-0003-4443-2473; Email: Sigurd.W.Loevseth@sintef.no

Authors

Dongchan Kim − *The University of Western Australia (M050), Perth WA 6009, Australia; Naval & Energy System R&D Institute, Energy System R&D Department, Daewoo Shipbuilding and Marine Engineering Co. Ltd. (DSME), Geoje-daero, Geoje-si, Gyeongsangnam-do 3370, Korea;* orcid.org/0000-0002-8345-3456

Arash Arami-Niya − *The University of Western Australia (M050), Perth WA 6009, Australia; Curtin University, Perth, WA 6845, Australia;* orcid.org/0000-0001-6450-0774

Eric F. May − *The University of Western Australia (M050), Perth WA 6009, Australia;* orcid.org/0000-0001-5472-6921

Complete contact information is available at: https://pubs.acs.org/10.1021/acs.jced.1c00270

Notes

The authors declare no competing financial interest.

ACKNOWLEDGMENTS

This publication has been produced with support from the research program CLIMIT and the NCCS Centre, performed under the Norwegian research program Centres for Environment-friendly Energy Research (FME). The authors acknowledge the following partners for their contributions: Aker Carbon Capture, Allton, Ansaldo Energia, Baker Hughes, CoorsTek Membrane Sciences, Equinor, Fortum Oslo Varme, Gassco, KROHNE, Larvik Shipping, Lundin Norway, Norcem, Norwegian Oil and Gas, Quad Geometrics, Stratum Reservoir, Total, Vår Energi, Wintershall DEA, the Research Council of Norway (257579/E20 and 280394), and the Australian Research Council (IC150100019).

REFERENCES

(1) *Global Warming of 1.5°C.*; IPCC, https://www.ipcc.ch/sr15/, 2018.

(2) *World Energy Outlook 2020*; International Energy Agency: Paris, France, 2020.

(3) Løvseth, S. W.; Skaugen, G.; Jacob Stang, H. G.; Jakobsen, J. P.; Wilhelmsen, Ø.; Span, R.; Wegge, R. CO_2Mix Project: Experimental Determination of Thermo Physical Properties of CO_2-Rich Mixtures. *Energy Procedia* **2013**, *37*, 2888−2896.

(4) Wang, J.; Ryan, D.; Anthony, E. J.; Wigston, A. *Effects of Impurities on Geological Storage of CO_2*; IEAGHG/Global CCS Institute: 2011.

(5) Tan, Y.; Nookuea, W.; Li, H.; Thorin, E.; Yan, J. Property Impacts on Carbon Capture and Storage (CCS) Processes: A Review. *Energy Convers. Manage.* **2016**, *118*, 204−222.

(6) IPCC. *IPCC Special Report on Carbon Dioxide Capture and Storage*; Intergovernmental Panel on Climate Change: Cambridge, UK, 2005.

(7) de Visser, E.; Hendriks, C.; Barrio, M.; Mølnvik, M. J.; de Koeijer, G.; Liljemark, S.; Le Gallo, Y. Dynamis CO_2 Quality Recommendations. *Int. J. Greenhouse Gas Control* **2008**, *2*, 478−484.

(8) Buit, L.; Ahmad, M.; Mallon, W.; Hage, F.; Zhang, X.; Koenen, M. *Standards for CO_2: Towards a transport infrastructure for large-scale CCS in Europe (CO_2Europipe)*; EU CO2Europipe Consortium: Netherlands, 2011.
(9) Matuszewski, M.; Woods, M. *CO_2 Impurity Design Parameters*; National Energy Technology Laboratory (NETL): USA, 2012.
(10) Noothout, P.; Wiersma, F.; Hurtado, O.; Roelofsen, P.; Macdonald, D. *CO_2 Pipeline Infrastructure*; Global CCS Institute, IEA Greenhouse Gas R&D Programme (IEAGHG), 2014.
(11) Brunsvold, A.; Jakobsen, J. P.; Mazzetti, M. J.; Skaugen, G.; Hammer, M.; Eickhoff, C.; Neele, F. Key Findings and Recommendations from the Impacts Project. *Int. J. Greenhouse Gas Control* **2016**, *54*, 588.
(12) Høydalsvik, H. *Gassnova CO_2 Capture, Transport and Storage - Mongstad CO_2 Product Specification*; Gassnova: Norway, 2013.
(13) Ackiewicz, M.; Mølnvik, M.; Løvseth, S. W.; Romanak, K.; Hovorka, S. *Technical Barriers and R&D Opportunities for Offshore, Sub-Seabed Geologic Storage of Carbon Dioxide*; Carbon Sequestration Leadership Forum (CSLF) Technical Group, 2015.
(14) *Feasibility Study for Full-Scale CCS in Norway*; Norwegian Ministry of Petroleum and Energy, Gassnova, Gassco, Statoil, 2016,https://ccsnorway.com/wp-content/uploads/sites/6/2019/09/feasibilitystudy_fullscale_ccs_norway_2016.pdf.
(15) Skaugen, G.; Roussanaly, S.; Jakobsen, J.; Brunsvold, A. Techno-Economic Evaluation of the Effects of Impurities on Conditioning and Transport of CO_2 by Pipeline. *Int. J. Greenhouse Gas Control* **2016**, *54*, 627.
(16) Knoope, M. M. J.; Ramírez, A.; Faaij, A. P. C. A State-of-the-Art Review of Techno-Economic Models Predicting the Costs of CO_2 Pipeline Transport. *Int. J. Greenhouse Gas Control* **2013**, *16*, 241−270.
(17) Li, H.; Jakobsen, J. P.; Wilhelmsen, Ø.; Yan, J. Pvtxy Properties of CO_2 Mixtures Relevant for CO_2 Capture, Transport and Storage: Review of Available Experimental Data and Theoretical Models. *Appl. Energy* **2011**, *88*, 3567−3579.
(18) Li, H.; Wilhelmsen, Ø.; Lv, Y.; Wang, W.; Yan, J. Viscosities, Thermal Conductivities and Diffusion Coefficients of CO_2 Mixtures: Review of Experimental Data and Theoretical Models. *Int. J. Greenhouse Gas Control* **2011**, *5*, 1119−1139.
(19) Gernert, J.; Span, R. EOS-CG: A Helmholtz Energy Mixture Model for Humid Gases and CCS Mixtures. *J. Chem. Thermodyn.* **2016**, *93*, 274−293.
(20) Munkejord, S. T.; Hammer, M.; Løvseth, S. W. CO_2 Transport: Data and Models − a Review. *Appl. Energy* **2016**, *169*, 499−523.
(21) Munkejord, S. T.; Hammer, M. Depressurization of CO_2-Rich Mixtures in Pipes: Two-Phase Flow Modelling and Comparison with Experiments. *Int. J. Greenhouse Gas Control* **2015**, *37*, 398−411.
(22) Lund, H.; Torsæter, M.; Munkejord, S. T. Study of Thermal Variations in Wells During Carbon Dioxide Injection. *SPE Drill. Completion* **2016**, *31*, 159.
(23) Goodarzi, S.; Settari, A.; Zoback, M. D.; Keith, D., *Thermal Aspects of Geomechanics and Induced Fracturing in CO_2 Injection with Application to CO_2 Sequestration in Ohio River Valley*; Society of Petroleum Engineers, 2010.
(24) de Koeijer, G.; Hammer, M.; Drescher, M.; Held, R. Need for Experiments on Shut-Ins and Depressurizations in CO_2 Injection Wells. *Energy Procedia* **2014**, *63*, 3022−3029.
(25) Berstad, D.; Anantharaman, R.; Nekså, P. Low-Temperature CO2 Capture Technologies − Applications and Potential. *Int. J. Refrig.* **2013**, *36*, 1403−1416.
(26) Nookuea, W.; Tan, Y.; Li, H.; Thorin, E.; Yan, J. Sensitivity Study of Thermo-Physical Properties of Gas Phase on Absorber Design for CO_2 Capture Using Monoethanolamine. *Energy Procedia* **2015**, *75*, 2305−2310.
(27) Vesovic, V.; Wakeham, W. A.; Olchowy, G. A.; Sengers, J. V.; Watson, J. T. R.; Millat, J. The Transport Properties of Carbon Dioxide. *J. Phys. Chem. Ref. Data* **1990**, *19*, 763−808.
(28) Huber, M. L.; Sykioti, E. A.; Assael, M. J.; Perkins, R. A. Reference Correlation of the Thermal Conductivity of Carbon Dioxide from the Triple Point to 1100 K and up to 200 MPa. *J. Phys. Chem. Ref. Data* **2016**, *45*, 013102.
(29) Lemmon, E. W.; Bell, I. H.; Huber, M. L.; McLinden, M. O. *Nist Standard Reference Database 23: Reference Fluid Thermodynamic and Transport Properties-Refprop*, version 9.1.1; National Institute of Standards and Technology, Standard Reference Data Program: Gaithersburg, USA, 2014.
(30) Chichester, J. C.; Huber, M. L. *Documentation and Assessment of the Transport Property Model for Mixtures Implemented in Nist Refprop (Version 8.0)*; National Institute of Standards and Technology (NIST): 2008.
(31) Ely, J. F.; Hanley, H. J. M. Prediction of Transport Properties - 2. Thermal Conductivity of Pure Fluids and Mixtures. *Ind. Eng. Chem. Fundam.* **1983**, *22*, 90−97.
(32) Wassiljewa, A. Wärmeleitungen in Gasgemischen. *Physikalisches Zeitschrift* **1904**, *5*, 737−742.
(33) Mason, E. A.; Saxena, S. C. Approximate Formula for the Thermal Conductivity of Gas Mixtures. *Phys. Fluids* **1958**, *1*, 361−369.
(34) Rosenfeld, Y. Relation between the Transport Coefficients and the Internal Entropy of Simple Systems. *Phys. Rev. A: At., Mol., Opt. Phys.* **1977**, *15*, 2545−2549.
(35) Lötgering-Lin, O.; Gross, J. Group Contribution Method for Viscosities Based on Entropy Scaling Using the Perturbed-Chain Polar Statistical Associating Fluid Theory. *Ind. Eng. Chem. Res.* **2015**, *54*, 7942−7952.
(36) Lötgering-Lin, O.; Fischer, M.; Hopp, M.; Gross, J. Pure Substance and Mixture Viscosities Based on Entropy Scaling and an Analytic Equation of State. *Ind. Eng. Chem. Res.* **2018**, *57*, 4095−4114.
(37) Bell, I. H. Probing the Link between Residual Entropy and Viscosity of Molecular Fluids and Model Potentials. *Proc. Natl. Acad. Sci. U. S. A.* **2019**, *116*, 4070−4079.
(38) Bell, I. H.; Messerly, R.; Thol, M.; Costigliola, L.; Dyre, J. C. Modified Entropy Scaling of the Transport Properties of the Lennard-Jones Fluid. *J. Phys. Chem. B* **2019**, *123*, 6345−6363.
(39) Bell, I. H.; Hellmann, R.; Harvey, A. H. Zero-Density Limit of the Residual Entropy Scaling of Transport Properties. *J. Chem. Eng. Data* **2020**, *65*, 1038−1050.
(40) Mylona, S. K.; Hughes, T. J.; Saeed, A. A.; Rowland, D.; Park, J.; Tsuji, T.; Tanaka, Y.; Seiki, Y.; May, E. F. Thermal Conductivity Data for Refrigerant Mixtures Containing R1234yf and R1234ze(E). *J. Chem. Thermodyn.* **2019**, *133*, 135−142.
(41) Mylona, S. K.; Yang, X.; Hughes, T. J.; White, A. C.; McElroy, L.; Kim, D.; Al Ghafri, S.; Stanwix, P. L.; Sohn, Y. H.; Seo, Y.; May, E. F. High-Pressure Thermal Conductivity Measurements of a (Methane + Propane) Mixture with a Transient Hot-Wire Apparatus. *J. Chem. Eng. Data* **2020**, *65*, 906−915.
(42) Kim, D.; Yang, X.; Arami-Niya, A.; Rowland, D.; Xiao, X.; Al Ghafri, S. Z. S.; Tsuji, T.; Tanaka, Y.; Seiki, Y.; May, E. F. Thermal Conductivity Measurements of Refrigerant Mixtures Containing Hydrofluorocarbons (Hfc-32, Hfc-125, Hfc-134a), Hydrofluoroolefins (Hfo-1234yf), and Carbon Dioxide (CO_2). *J. Chem. Thermodyn.* **2020**, *151*, 106248.
(43) De Groot, J. J.; Kestin, J.; Sookiazian, H. Instrument to Measure the Thermal Conductivity of Gases. *Physica* **1974**, *75*, 454−482.
(44) Healy, J. J.; de Groot, J. J.; Kestin, J. The Theory of the Transient Hot-Wire Method for Measuring Thermal Conductivity. *Physica B+C* **1976**, *82*, 392−408.
(45) Mason, E. A.; Khalifa, H. E.; Kestin, J.; DiPippo, R.; Dorfman, J. R. Composition Dependence of the Thermal Conductivity of Dense Gas Mixtures. *Phys. A* **1978**, *91*, 377−392.
(46) Kestin, J.; Wakeham, W. A. A Contribution to the Theory of the Transient Hot-Wire Technique for Thermal Conductivity Measurements. *Phys. A* **1978**, *92*, 102−116.
(47) Roder, H. M. A Transient Hot Wire Thermal Conductivity Apparatus for Fluids. *J. Res. Natl. Bur. Stand.* **1981**, *86*, 457−493.
(48) Perkins, R. A.; Roder, H. M.; de Castro, C. A. N. A High-Temperature Transient Hot-Wire Thermal-Conductivity Apparatus for Fluids. *J. Res. Natl. Inst. Stand. Technol.* **1991**, *96*, 247−269.

https://doi.org/10.1021/acs.jced.1c00270
J. Chem. Eng. Data XXXX, XXX, XXX−XXX

(49) Woodfield, P. L.; Moroe, S.; Fukai, J.; Fujii, M.; Shinzato, K.; Kohno, M.; Takata, Y. Techniques for Accurate Resistance Measurement in the Transient Short-Hot-Wire Method Applied to High Thermal-Diffusivity Gas. *Int. J. Thermophys.* **2009**, *30*, 1748.
(50) Moroe, S.; Woodfield, P. L.; Kimura, K.; Kohno, M.; Fukai, J.; Fujii, M.; Shinzato, K.; Takata, Y. Measurements of Hydrogen Thermal Conductivity at High Pressure and High Temperature. *Int. J. Thermophys.* **2011**, *32*, 1887.
(51) Antoniadis, K. D. Measurement of the Thermal Conductivity of Composite Solid Materials. Ph.D. Thesis, Aristotle University of Thessaloniki, Thessaloniki, Greece, 2011.
(52) Kunz, O.; Klimeck, R.; Wagner, W.; Jaeschke, M. *The GERG-2004 Wide-Range Equation of State for Natural Gases and Other Mixtures.*; VDI Verlag: Düsseldorf, Germany, 2007; *Vol. 15*.
(53) Span, R.; Wagner, W. A New Equation of State for Carbon Dioxide Covering the Fluid Region from the Triple-Point Temperature to 1100 K at Pressures up to 800 MPa. *J. Phys. Chem. Ref. Data* **1996**, *25*, 1509−1596.
(54) Span, R.; Lemmon, E. W.; Jacobsen, R. T.; Wagner, W.; Yokozeki, A. A Reference Equation of State for the Thermodynamic Properties of Nitrogen for Temperatures from 63.151 to 1000 K and Pressures to 2200 MPa. *J. Phys. Chem. Ref. Data* **2000**, *29*, 1361−1433.
(55) van Dusen, M. S. Platinum-Resistance Thermometry at Low Temperatures. *J. Am. Chem. Soc.* **1925**, *47*, 326−332.
(56) Carslaw, H. S.; Jaeger, J. C. *Conduction of Heat in Solids.*, 2nd ed.; Oxford University Press: Oxford, UK, 1959.
(57) Fischer, J. Zur Bestimmung Der Wärmeleitfähigkeit Und Der Temperaturleitfähigkeit Aus Dem Ausgleichvorgang Beim Schleiermacherschen Meßrohrverfahren Und Beim Plattenverfahren. *Ann. Phys.* **1939**, *426*, 669−688.
(58) de Castro, C. A. N.; Li, S. F. Y.; Maitland, G. C.; Wakeham, W. A. Thermal Conductivity of Toluene in the Temperature Range 35−90°C at Pressures up to 600 MPa. *Int. J. Thermophys.* **1983**, *4*, 311−327.
(59) *NIST Literature Report Builder for Thermophysical and Thermochemical Property Measurements*; National Institue of Standards and Technology, 2014.
(60) Crusius, J.-P.; Hellmann, R.; Castro-Palacio, J. C.; Vesovic, V. Ab Initio Intermolecular Potential Energy Surface for the CO_2—N_2 System and Related Thermophysical Properties. *J. Chem. Phys.* **2018**, *148*, 214306.
(61) Johns, A. I.; Rashid, S.; Rowan, L.; Watson, J. T. R.; Clifford, A. A. The Thermal Conductivity of Pure Nitrogen and of Mixtures of Nitrogen and Carbon Dioxide at Elevated Temperatures and Pressures. *Int. J. Thermophys.* **1988**, *9*, 3−19.
(62) K. Barua, A.; Manna, A.; Mukhopadhyay, P. Erratum: "Thermal Conductivity of Argon-Carbondioxide and Nitrogen-Carbondioxide Gas Mixtures. *J. Phys. Soc. Jpn.* **1969**, *26*, 588−588.
(63) K. Barua, A.; Manna, A.; Mukhopadhyay, P. Thermal Conductivity of Argon-Carbondioxide and Nitrogen-Carbondioxide Gas Mixtures. *J. Phys. Soc. Jpn.* **1968**, *25*, 862−867.
(64) Gilmore, T. F.; Comings, E. W. Thermal Conductivity of Binary Mixtures of Carbon Dioxide, Nitrogen, and Ethane at High Pressures: Comparison with Correlation and Theory. *AIChE J.* **1966**, *12*, 1172−1178.
(65) Westenberg, A. A.; DeHaas, N. Gas Thermal-Conductivity Studies at High Temperature. Line-Source Technique and Results in N_2, CO_2, and N_2-CO_2 Mixtures. *Phys. Fluids* **1962**, *5*, 266−273.
(66) Cheung, H.; Bromley, L. A.; Wilke, C. R. Thermal Conductivity of Gas Mixtures. *AIChE J.* **1962**, *8*, 221−228.
(67) Vines, R. G. Measurement of the Thermal Conductivities of Gases at High Temperatures. *J. Heat Transfer* **1960**, *82*, 48−52.
(68) von Lehmann, H. Wärmeleitfähigkeit Von Gasgemischen. *Chem. Technol. (Leipzig)* **1957**, *9*, 530−537.
(69) Kulakov, I. A. Izv. Voronezh Pedagogical Institute, (17), 1955.
(70) Rothman, A. J.; Bromley, L. A. High Temperature Thermal Conductivity of Gases. *Ind. Eng. Chem.* **1955**, *47*, 899−906.
(71) Rothman, A. J. *Thermal Conductivity of Gases at High Temperatures*; University of California, Berkeley: Berkeley, CA, USA, 1954.
(72) Davidson, J. M.; Music, J. F. *Experimental Thermal Conductivities of Gases and Gaseous Mixtures at Zero Degrees Centigrade*; USA Atomic Energy Commission, 1953,https://play.google.com/books/reader?id=Somen40fqdkC.
(73) Keyes, F. G.; Mass, C. Additional Measurements of Heat Conductivity of Nitrogen, Carbon Dioxide, and Mixtures. *Trans. ASME* **1952**, *74*, 1303−1306.
(74) Keyes, F. G. Measurements of the Heat Conductivity of Nitrogen-Carbon Dioxide Mixtures. *Trans. ASME* **1951**, *73*, 597−603.
(75) Hellmann, R.; Bich, E.; Vesovic, V. Cross Second Virial Coefficients and Dilute Gas Transport Properties of the (CH_4+CO_2), (CH_4+H2S), and (H_2S+CO_2) Systems from Accurate Intermolecular Potential Energy Surfaces. *J. Chem. Thermodyn.* **2016**, *102*, 429−441.
(76) Pátek, J.; Klomfar, J.; Čapla, L.; Buryan, P. Thermal Conductivity of Carbon Dioxide−Methane Mixtures at Temperatures between 300 and 425 K and at Pressures up to 12 mpa. *Int. J. Thermophys.* **2005**, *26*, 577−592.
(77) Yorizane, M.; Yoshimura, S.; Masuoka, H.; Yoshida, H. Thermal Conductivities of Binary Gas Mixtures at High Pressures: Nitrogen-Oxygen, Nitrogen-Argon, Carbon Dioxide-Argon, and Carbon Dioxide-Methane. *Ind. Eng. Chem. Fundam.* **1983**, *22*, 458−463.
(78) Kestin, J.; Ro, S. T.; Nagasaka, Y. The Thermal Conductivity of Mixtures of Methane with Carbon Dioxide. *Berichte der Bunsengesellschaft für physikalische Chemie* **1982**, *86*, 945−948.
(79) Christensen, P. L.; Fredenslund, A. Thermal Conductivity of Gaseous Mixtures of Methane with Nitrogen and Carbon Dioxide. *J. Chem. Eng. Data* **1979**, *24*, 281−283.
(80) Rosenbaum, B. M.; Thodos, G. Thermal Conductivity of Mixtures in the Dense Gaseous State: The Methane−Carbon Dioxide System. *J. Chem. Phys.* **1969**, *51*, 1361−1368.
(81) *Evaluation of Measurement Data—Guide to the Expression of Uncertainty in Measurement (Gum)*; Joint Committee for Guides in Metrology, 2008.
(82) Herrig, S. *New Helmholtz-Energy Equations of State for Pure Fluids and CCS-Relevant Mixtures*. Ph.D. Dissertation, Ruhr-Universität Bochum, 2018.
(83) Setzmann, U.; Wagner, W. A New Equation of State and Tables of Thermodynamic Properties for Methane Covering the Range from the Melting Line to 625 K at Pressures up to 100 MPa. *J. Phys. Chem. Ref. Data* **1991**, *20*, 1061−1155.

https://doi.org/10.1021/acs.jced.1c00270
J. Chem. Eng. Data XXXX, XXX, XXX−XXX